Computers in Biology and Medicine 190 (2025) 109994

Contents lists available at ScienceDirect

Computers in Biology and Medicine

journal homepage: www.elsevier.com/locate/compbiomed

Enhancing premature ventricular contraction localization through electrocardiographic imaging and cardiac digital twins

Jorge Sánchez [a,*], Inés Llorente-Lipe [a], Cristian Barrios Espinosa [b], Axel Loewe [b], Ismael Hernández-Romero [a,d], Jorge Vicente-Puig [d,e], Santiago Ros [a,c,f], Felipe Atienza [c,d,f,g], Alejandro Carta-Bergaz [c,f], Andreu M. Climent [a,d], Maria S. Guillem [a,d]

[a] Universitat Politècnica de València, Camíde Vera s/n, Valencia, 46022, Spain
[b] Institute of Biomedical Engineering, Karlsruhe Institute of Technology (KIT), Kaiserstr. 12, Karlsruhe, 76131, Germany
[c] Department of Cardiology, Hospital General Gregorio Marañón, Instituto de Investigación Sanitaria Gregorio Marañón (IISGM), C. del Dr. Esquerdo, 46, Marid, 28007, Spain
[d] Corify Care SL., Calle del Dr. Castelo, 44, Bajo Izquierda, Marid, 28009, Spain
[e] Departament de Matematiques, Universitat Autonoma de Barcelona, Bellaterra, Barcelona, 08193, Spain
[f] Center for Biomedical Research in Cardiovascular Disease Network (CIBERCV), Av. Monforte de Lemos, 3-5. Pabellón 11, Marid, 28029, Spain
[g] Universidad Complutense de Madrid, Av. Complutense, s/n, Moncloa - Aravaca, Marid, 28040, Spain

ARTICLE INFO

Keywords:
ECGI
Digital twins
PVC
Computer modeling
Therapy personalization

ABSTRACT

Premature ventricular contractions (PVCs) represent a common and clinically significant cardiac arrhythmia, contributing to a spectrum of cardiovascular disorders. Accurate localization of the origin of PVCs is essential for devising targeted therapeutic strategies and refining our comprehension of ventricular arrhythmogenesis. Traditionally, the 12-lead ECG has been the go-to diagnostic tool for PVCs. However, individual anatomical differences and inter-patient electrophysiology variability limit its effectiveness. This study presents a new method that combines electrocardiographic imaging (ECGI) with the concept of cardiac digital twins (ECGI-DT) to improve the accuracy of pinpointing the source of PVCs. By simulating a database of PVCs, we developed an ECGI-DT capable of estimating the origins of PVCs with much greater precision than possible previously. This study shows a notable improvement in identifying the initial site of PVC origin using ECGI-DT compared to ECGI alone: the average localization error dropped from 30.69 ± 23.71 mm with standard ECGI to 7.81 ± 3.82 mm using the ECGI-DT method. This marked reduction in error highlights the potential of ECGI-DT in revolutionizing PVC diagnosis and treatment. With its ability to provide more accurate and reliable data, ECGI-DT could improve the planning of catheter ablation treatments, a preferred intervention for managing PVCs that face challenges such as high costs and in some cases long procedure times.

1. Introduction

Premature ventricular contractions (PVCs) are common and occur with an estimated prevalence of 40% to 75% [1] in general population, which increases with age and comorbidity burden [2]. Although considered benign in general population [1], highly symptomatic patients require therapy [3]. PVCs originated in the outflow tract can cause ventricular arrhythmias, which are the most common type of idiopathic ventricular arrhythmias, accounting for approximately 70% of cases [4–6]. However, idiopathic PVCs that originate from the left ventricular septum, not involving the left anterior or posterior fascicle, have also been observed [7]. Moreover, some patients develop cardiomyopathy and under certain conditions PVCs may trigger ventricular arrhythmias [8,9].

The preferred treatment for PVCs is catheter ablation, which consists in creating a non-conducting scar in the tissue from which PVCs arise [10]. Clinically, the precise localization of PVC origins is crucial for determining the most effective ablation strategy. For planning a catheter ablation strategy, the site of origin—whether epicardial or endocardial or located in the right or left ventricle—significantly influences the approach and procedure planning. Moreover, catheter

* Corresponding author.
E-mail addresses: jorsana4@itaca.upv.es (J. Sánchez), inlloli@itaca.upv.es (I. Llorente-Lipe), cristian.espinosa@kit.edu (C.B. Espinosa), axel.loewe@kit.edu (A. Loewe), isherro@itaca.upv.es (I. Hernández-Romero), jorge.vicente@corifycare.com (J. Vicente-Puig), santiago.ros@mc.iisgm.com (S. Ros), felipe.atienza@salud.madrid.org (F. Atienza), alejandro.carta@salud.madrid.org (A. Carta-Bergaz), acliment@itaca.upv.es (A.M. Climent), mguisan@itaca.upv.es (M.S. Guillem).

https://doi.org/10.1016/j.compbiomed.2025.109994
Received 26 July 2024; Received in revised form 1 February 2025; Accepted 4 March 2025
Available online 22 March 2025

ablation is an expensive treatment, can take more than 130 min, and exposes the patients to radiation due to the fluoroscopy needed to guide the procedure [11–13].

Currently, PVCs can be diagnosed using the 12-lead ECG [4]. However, the rule-based decision algorithms to locate the PVC origin require accurate measurement of 12-lead ECG intervals and R/S voltage relation, posing challenges for practical and reproducible implementation [4]. Moreover, Penela et al. showed that rule-based decision algorithms can be improved by combining clinical and 12-lead ECG markers to predict the origin of the PVC [14]. Furthermore, diagnostics based on signals can be impaired by variations in torso anatomy, heart orientation, and lead placement.

In recent years, electrocardiographic imaging (ECGI) has emerged as an alternative method to guide ablation treatments. ECGI has been shown to help determine the location of PVCs. Previous work explored the use of ECGI inverse solutions [15–19] or artificial intelligence to locate PVCs [20–22]. However, ECGI lacks the precision to determine the exact location of PVCs [16,23] and local activation time (LAT) maps calculation is prone to artificial lines of block [23–25].

Nowadays, computer models allow creating personalized representations of a patient's cardiac electrophysiology, so-called digital twins [26]. Thanks to the personalized model, information about the electrical propagation dynamics can be obtained and used to suggest personalized treatments. Several groups have shown the capabilities of computer models to generate a digital twin [27–29]. Moreover, eikonal simulations are a computationally efficient way to simulate the propagation of the excitation of the myocardium [30,31]. Body surface potential maps (BSPM) can be computed using a bidomain model [32,33]. However, solving the bidomain model is computationally expensive due to the high accuracy in simulate BSPMs, and combining eikonal simulations with volume conductor solved using a boundary element method approach has been proposed to compute the BSPM in a fast and accurate way [27,34,35].

Therefore, in this study, we combine ECGI by using the LAT map, with ventricular digital twins (ECGI-DT) to simulate the PVC propagation that reproduce the potentials at the surface of the torso, offering increased precision in localizing the origin of PVCs compared to ECGI-only estimation. We created a database of simulated PVCs to develop and obtain an ECGI-DT that estimates the PVC origin. Additionally, we provide information on the myocardium propagation and activation times maps with no artificial line of blocks.

2. Materials and methods

The proposed ECGI-DT methodology departs from a LAT map obtained with ECGI and 128 signals acquired at the surface of the torso. ECGI-DT comprises four components, which together allow estimating the origin of a PVC from non-invasive measurements. First, we created a patient-specific database of PVC simulations explained in Sections 2.1 and 2.2. Second, a decision-making algorithm explained in Section 2.3 performs an estimation of the PVC location. Third, eikonal simulations and body surface potential forward calculations are run to obtain a LAT map and BSPM. From the BSPM simulation, the precordial leads are compared against the input BSPM precordial leads signals. If the mean Pearson's correlation is above 0.8, the location is accepted as the origin of the PVC. If the mean Pearson's correlation coefficient is below 0.8, an optimization of the PVC location is triggered. The complete workflow is depicted in Fig. 1, and each step is described in more detail below. The ECGI-DT was developed in Python, and the code is available on a Github repository.

2.1. Electrophysiology modeling

We created anatomically detailed meshes derived from 3D reconstruction of the torso and a biventricular statistical shape model [36]. The torso model and the 128 electrode positions were obtained with the Acorys system (Corify Care S.L.) using photogrammetry techniques that allow 3D reconstruction of the torso [37]. The biventricular detailed model corresponds to the mean shape from the statistical shape model of [36]. The ventricles were positioned inside the torso according to anatomical constraints [38] as well as lungs, blood pool, and liver to incorporate torso heterogeneities to reproduce a physiological BSPM [32]. The extracellular medium was considered isotropic, and conductivity for the blood, lungs, liver, and torso were 0.7 S/m, 0.0389 S/m, 0.1667 S/m, and 0.8 S/m, respectively [32,38]. The ventricular geometry was processed to add preferred myocyte orientation using a rule-based method [39]. Additionally, functional regions were added to the ventricular myocardium to set the conduction velocity (CV) to 2.0 m/s in a fast endocardial layer [40] and 0.7 m/s [41] for the mid-myocardium and epicardium with an anisotropy ratio of 3:1. CV was achieved by adjusting the intracellular and extracellular conductivities as described by Costa et al. [42]. Human cellular ventricular electrophysiology was simulated using the mathematical model proposed by Tomek et al. [43]. The ionic model was paced 100 times at basic cycle length of 1000 ms to reach a limit cycle. Furthermore, the mesh had an average edge length of 350 μm. The bidomain model was solved using openCARP [44,45] to simulate the electrical propagation in the ventricular myocardium and the electrical fields across the torso. Moreover, eikonal simulations were run to obtained the propagation in the myocardium based on the new estimated coordinate of the PVC in a coarser mesh with 600 μm average edge length [31,46,47]. Additionally, eikonal simulations were also used to fine-tune the location of the PVC. To accelerate the computation of eikonal simulations, the action potential model proposed by Mitchell & Schaeffer [48] was used.

2.2. Forward and inverse problem modeling

Body surface potentials from the eikonal simulations were obtained using the algorithms described by Stenroos et al. with a homogeneous conductor and the boundary element method [35,49,50]. Additionally, as suggested by Schuler et al. [51], action potentials from the eikonal simulations were spatially smoothed to compute the BSPM. To calculate ECGI, a reduced surface mesh of the ventricular myocardium was extracted with an average edge length of 2.8 mm [51] and a torso surface with an average edge length of 23 mm. Additionally, a set of 128 virtual electrodes at the torso surface was used to estimate the PVC origin and create the ventricular digital twin. The inverse problem of electrocardiography was solved using an equivalent single layer source model and zero-order Tikhonov regularization to recover the extracellular endocardial and epicardial potentials [52]. The L-curve criterion was used to choose the regularization parameter [53]. ECGI LAT maps were calculated by transforming each reconstructed extracellular potential at the ventricular surface as a sum of sinusoidal wavelets for all the negative slope time samples and amplitude proportional to the slope at that time and selecting the instant of the maximum amplitude of the transformed signal as the instant of activation time [54,55].

2.3. Estimating the PVC origin

To enhance the information ECGI provides, we created a database that consists of 618 bidomain simulations of PVCs (Section 2.1). Premature beats were distributed in the detailed ventricular geometry using an extended version of the Cobiveco coordinate system [56]. Briefly, we added a set of additional labels at the base of the detailed ventricular geometry in order to be able to compute the Cobiveco coordinates. We also introduced a scalar field at the left and right ridge to make it possible to locate points at these locations (Appendix A.11). The proposed algorithm, depicted in Fig. 2 compares the LAT map from the ECGI with the LAT maps available in the database. The four simulations from the database that exhibit the highest Pearson's correlation coefficient (CC) of the LAT maps are selected. Subsequently,

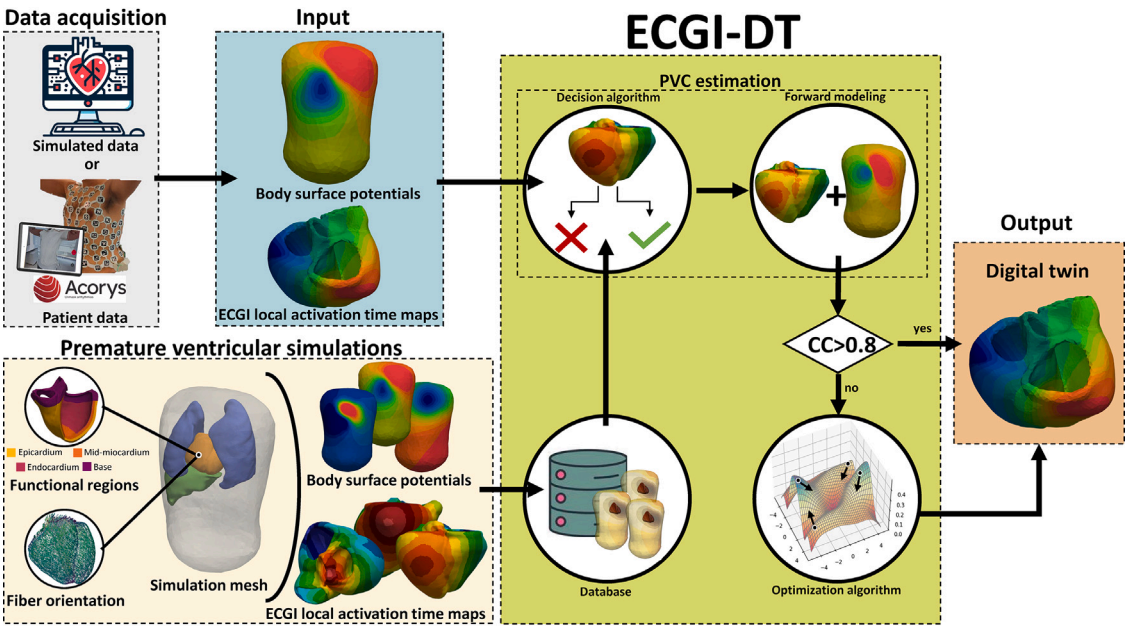

Fig. 1. ECGI-DT workflow with inputs ECGI LAT map and BSPM. The inputs for the proposed ECGI-DT are a BSPM and an ECGI LAT map. ECGI-DT comprises four components: a database of 618 PVC bidomain model simulations from which BSPM and ECGI LAT maps were calculated. A decision-making algorithm provides an estimated PVC location to compute a solution to the forward problem. Forward modeling comprises eikonal simulations and computation of the body surface potentials using a homogeneous volume conductor and the boundary element method. Lastly, the final digital twin is accepted if a mean Pearson's correlation coefficient is obtained. Otherwise, an optimization algorithm is used for fine-tuning the PVC location.

the BSPMs of these chosen models are evaluated against the measured body surface potentials, and only those simulations with a body surface potential CC greater than 0.7 proceed to the decision-making algorithm.

The decision-making algorithm takes as input the best simulations from the database to start the estimation of the PVC origin. The algorithm evaluates the transmural coordinates to identify if the PVC comes from the endocardial or epicardial site. The algorithm checks the occurrence of the transmural coordinate and takes the mode of the highest occurrence. Then, the rotational coordinate is evaluated. If the rotational coordinate is between 0.0 and 0.7, it means that the PVC origin is considered to be located at the free wall; otherwise, it is assumed to be located at the septum. The rotational coordinate is estimated by taking the median. Then, for the apicobasal coordinate, the median is taken, and for the transventricular coordinate, the mode. Then, the transversal scalar field added to Cobiveco is evaluated to identify if the origin of the PVC is in the aortic ridge or the right ventricular ridge. The output of the decision algorithm is a set of coordinates which indicate the estimate location of the PVC origin used later in the forward modeling step.

2.4. Forward model, optimization and PVC estimation

Finally, the estimated coordinate is used to run an eikonal simulation and then estimate the projected BSPM. From the simulated BSPM, the precordial leads were used to calculate the mean CC with respect to input data. If the mean CC is less than 0.8, a particle swarm optimization algorithm [57] is used to fine-tune the estimated coordinate. The particle swarm optimization was initialized with 4 particles and stopped when the precordial leads achieved a mean CC above 0.8 or after a maximum of 10 iterations.

2.5. Evaluation

The proposed algorithm was evaluated against an independent set of 75 additional bidomain simulations outside the database with a CV for the myocardium of 0.7 m/s, which will serve as the ground truth of the PVC origin. The test set was composed of 15 PVCs located at the RV free wall (7 epicardial and 8 endocardial), 15 PVCs located at the LV free wall (7 epicardial and 8 endocardial), 20 PVCs located at the septum, and 25 PVCs located at the ventricular base. Moreover, the evaluation set included a total of 300 additional bidomain simulation with four different myocardial conduction velocities of 1.0, 0.8, 0.6, and 0.4 m/s to test the proposed algorithm's robustness against variability of CV. CV of the fast endocardial layer was kept at 2.0 m/s for all cases. CV robustness was calculated by obtaining the variance coefficient of the mean error for ECGI and ECGI-DT. In addition, ECGI-DT was tested by adding white Gaussian noise to the BSPM with different signal to noise ratio (SNR) and filtered using a lowpass filter with a cut-off value of 60 Hz. Then, the inverse problem was compute to obtain the LAT at the ventricular surface. SNR was varied from 40 dB to 0 dB. The error of the PVC location was calculated by detecting the earliest activation site (EAS) in both ECGI and ECGI-DT LAT maps. The EAS was determined by obtaining the area of the LAT map which was activated at the earliest 2.5 percentile in LATs. From the largest earliest activated area the centroid was obtained and used as the EAS. Then, the Euclidean and geodesic distance were calculated between the ground truth and ECGI or ECGI-DT EAS in a tetrahedral mesh based on the A* algorithm [58] using NetworkX [59]. Geodesic distances are proposed due to the complex ventricular anatomy, which has convex and concave regions, which the Euclidean distance will not discriminate, especially near the apex and between the septum and the free wall of the right and left ventricles. The mean error is reported using the geodesic distance unless stated differently.

To evaluate the LAT maps of ECGI and ECGI-DT we propose to obtain the LAT isochrones using a geometric common ratio of 1.1 to obtain homogeneous separation between isochrones. The homogeneous separation of isochrones help to obtain a similar number of isochrones between LAT maps. The Euclidean distance between isochrones points was calculated, and the distance measurements were distributed in 50 bins. The ratio between the maximum number of samples in the minimum distance of the ECGI LAT map and the ECGI-DT LAT map was calculated with respect to the ground truth LAT map.

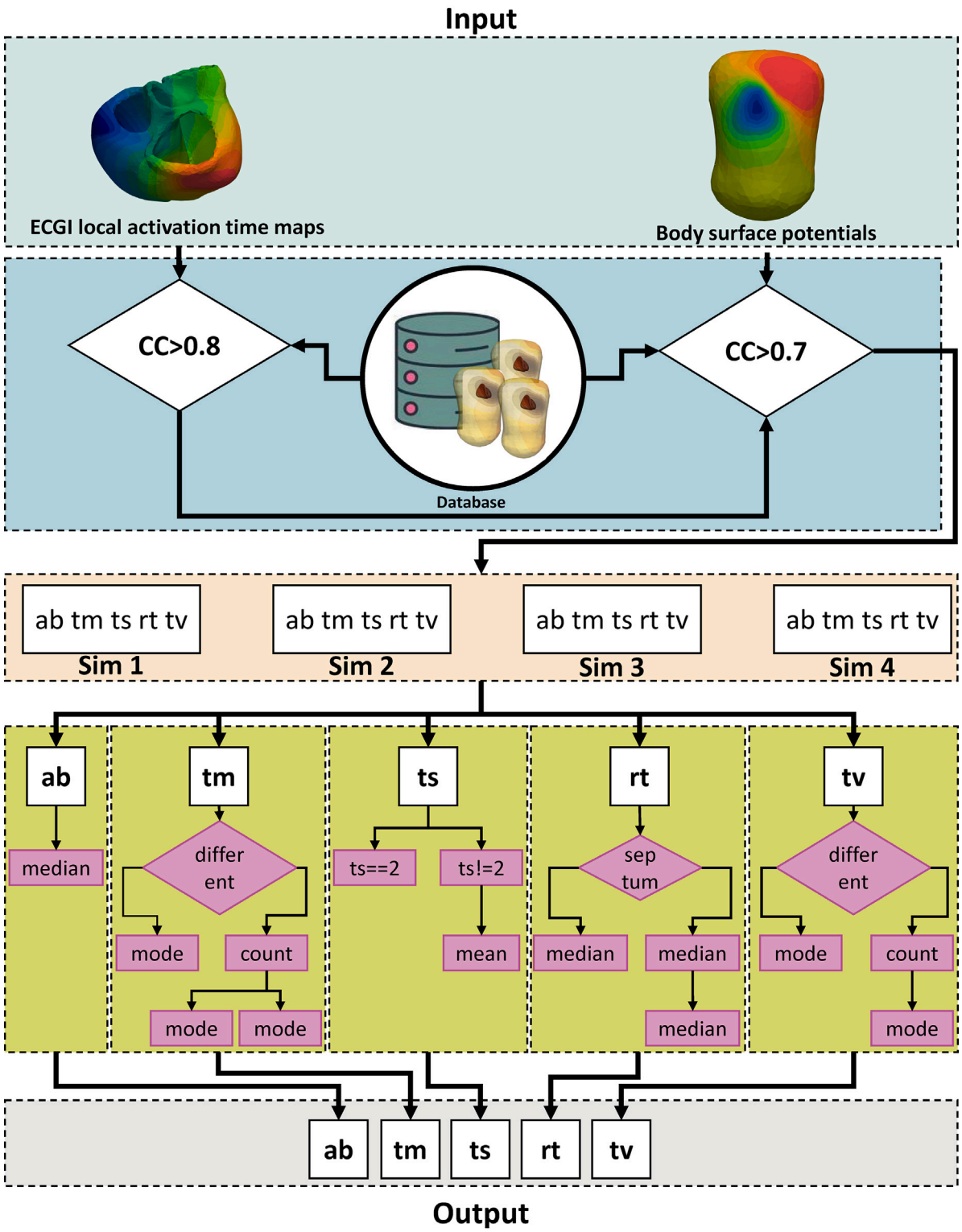

Fig. 2. Algorithm description to estimate the PVC origin. The location are coded using the extended Cobievo system. Transventricular coordinate (tv), apicobasal coordinate (ab), transmural coordinate (tm), rotational coordinate (rt), and transversal field (ts).

2.6. Clinical data

This study included a 42 years old female patient recruited at Hospital Gregorio Marañón (Madrid, Spain) diagnosed with PVC at the left ventricular free wall. Electroanatomical maps were acquired during sinus rhythm using the CARTO3 mapping system (Biosense Webster) with a 20-pole PentaRay catheter (Biosense Webster). The study was approved by the Institutional Review Board of Universitat Politecnica

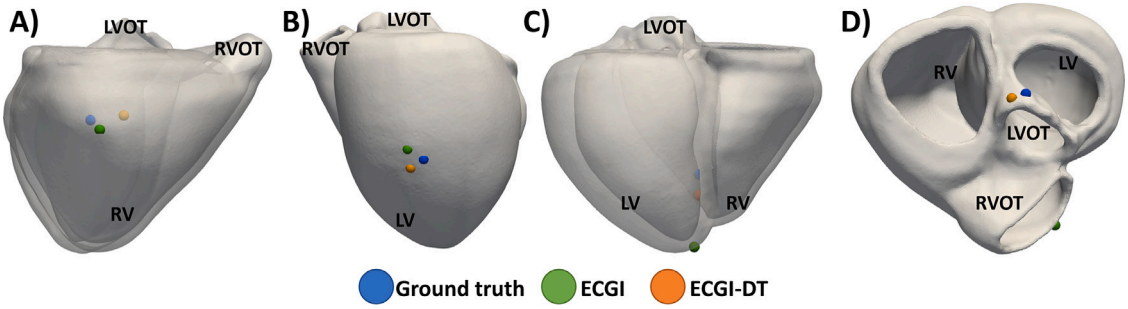

Fig. 3. PVC origin for four different scenarios. PVC of ground truth (blue circle), ECGI (green circle), and ECGI-DT (orange circle).

de Valencia and Hospital Gregorio Marañón (protocol code "SAVE-COR" approved on 02.06.2022) and in accordance with the Helsinki declaration. The patient gave written informed consent.

3. Results

The proposed ECGI-DT methodology allowed a correct identification of the chamber (right vs. left) and depth (epi vs. endo) of the PVCs for all the simulations of the evaluation set. ECGI-DT correctly identify the chamber in 100% of the cases vs. 75% using ECGI. Additionally, ECGI identify the PVC depth in 69% of the cases at the epicardial site even for PVCs located at the septum.

3.1. ECGI-DT earliest activation site location

Performance of the ECGI-based EAS identification showed a strong dependency on the location of the true initiation site. To illustrate this dependency examples of the performance of the proposed algorithm on four different cases are shown in Fig. 3. For a PVC originating from the right ventricular free wall, ECGI allowed an estimation of the EAS with a geodesic error of 7.17 mm (Fig. 3 panel A). ECGI located the PVC at the epicardial site, while ECGI-DT located the PVC correctly at the endocardial site with an error of 12.31 mm. For the free wall of the left ventricle, ECGI had an error of 31.15 mm, while ECGI-DT had an error of 6.89 mm (Fig. 3 panel B). At the septal region, ECGI had an error of 41.22 mm, while ECGI-DT had an error of 11.37 mm (Fig. 3 panel C). On the base of the ventricle, ECGI had an error of 60.10 mm, while ECGI-DT had an error of 5.24 mm (Fig. 3 panel D).

Globally, the accuracy of the ECGI-based EAS estimation was 30.69 ± 23.71 mm vs. 7.73 ± 3.71 mm with the proposed ECGI-DT algorithm. Additionally, the global Euclidean accuracy of the ECGI-based EAS estimation was 21.26 ± 12.77 mm vs. 6.35 ± 2.86 mm with the proposed ECGI-DT algorithm. The main difference between using Euclidean and geodesic distance was found in the ECGI-based estimation at the septal area. The ECGI-based estimation accuracy at the septal area using Euclidean distance was 29.82 ± 13.71 mm compared to 49.31 ± 25.44 mm using geodesic distance. Estimation errors for both ECGI and ECGI-DT are shown in Fig. 5, grouped into RV free wall, LV free wall, septum and base regions. Accuracy of ECGI-based EAS estimation was higher in both right and left free walls, with errors of 13.19 ± 7.45 mm and 22.45 ± 19.51 mm than for the septum and ventricular base, with errors of 47.65 ± 29.24 mm and 37.15 ± 17.98 mm. Errors in the ECGI-DT were always smaller both in the mean and standard deviation values, more independent on the location of the stimulation site with values of 7.57 ± 2.96 mm for the RV free wall, 6.14 ± 2.74 mm for the LV free wall, 9.28 ± 4.81 mm for the septum, and 9.45 ± 4.17 mm for the base.

3.2. ECGI-DT LAT pattern estimation

ECGI-DT not only allowed an improved estimation of the EAS, but also an improved estimation of the LATs in the entire myocardium, as it can be observed in Fig. 4. In general, the EAS in the ECGI-DT LAT map is better identified than ECGI LAT maps where the EAS is larger than the ground truth EAS LAT map. EAS located at the ventricular base are overestimated by ECGI (Fig. 4 panel D) compared to the ground truth EAS. Notice that both the total activation time and the location of the latest activation site were better estimated on the ECGI-DT. Fig. 6 shows the difference of LAT between ground truth, ECGI, and ECG-DT. The maximum absolute error for ECGI-DT LAT maps was below 15 ms for the four PVCs cases shown as example, while the maximum absolute error for ECGI LAT maps ranged from 74 ms to 111 ms. The difference in LATs was observed at the base of the ventricle in the LVOT (Fig. 6 panel D). Additionally, the mean error in LAT estimation of ECGI-DT was 2.62 ± 5.42 ms, 2.13 ± 5.11 ms, 0.58 ± 7.28 ms, and 6.37 ± 9.23 ms for RV free wall, LV free wall, septum, and base, respectively.

ECGI-DT allowed to reduce the presence of artificial block lines that appear in potential-based ECGI solutions [51]. To estimate this reduction in the presence of artificial block lines, we quantified, in four scenarios, the isochronal density both in ECGI and ECGI-DT LAT maps (Fig. 7). At the PVC origin we found a high density of isochrones (0.17 ± 0.08 isochrones per mm) in the "ground truth" simulations, which may indicate a real slow conduction that can be attributed to a source–sink mismatch effect coming from the small volume of activating tissue compared to the myocardium volume to be activated. In contrast, ECGI LAT maps present a higher density of isochrones than the ground truth and ECGI-DT. For a PVC located at the RV free wall, the ratio of isochrones distance between ECGI and ground truth was 2.20 (Fig. 7 panel A), while the ECGI-DT ratio was 0.55. Higher isochrone density was observed for PVCs located at the LV free wall (Fig. 7 panel B), septum (Fig. 7 panel C), and the LVOT (Fig. 7 panel D) with 9.38, 9.21, and 9.38 compared to the ECGI-DT ratio of 0.64, 0.58, and 1.15 for LV free wall, septum, and LVOT.

3.3. ECGI-DT algorithm performance

The particle swarm optimization algorithm needed a maximum of 3 iterations with 4 particles. An initial estimation of the PVC location could be achieved in ~3 min using a desktop computer with an AMD Ryzen Threadripper PRO 5995WX CPU. For the fine-tuning step, the total computation time was ~35 min to obtain the ventricular digital twin, which provided a LAT map with a coherent activation sequence compared to the LAT map from ECGI alone (Fig. 4).

ECG tracings in the BSPM signals estimated from the ECGI-DT were very similar to those from the "ground truth" with a mean CC of 0.80 for the precordial leads of the ECG, which allowed reproducing the depolarization pattern arising by a PVC at the ventricular myocardium and the potentials at the torso surface (Supplemental material Fig.

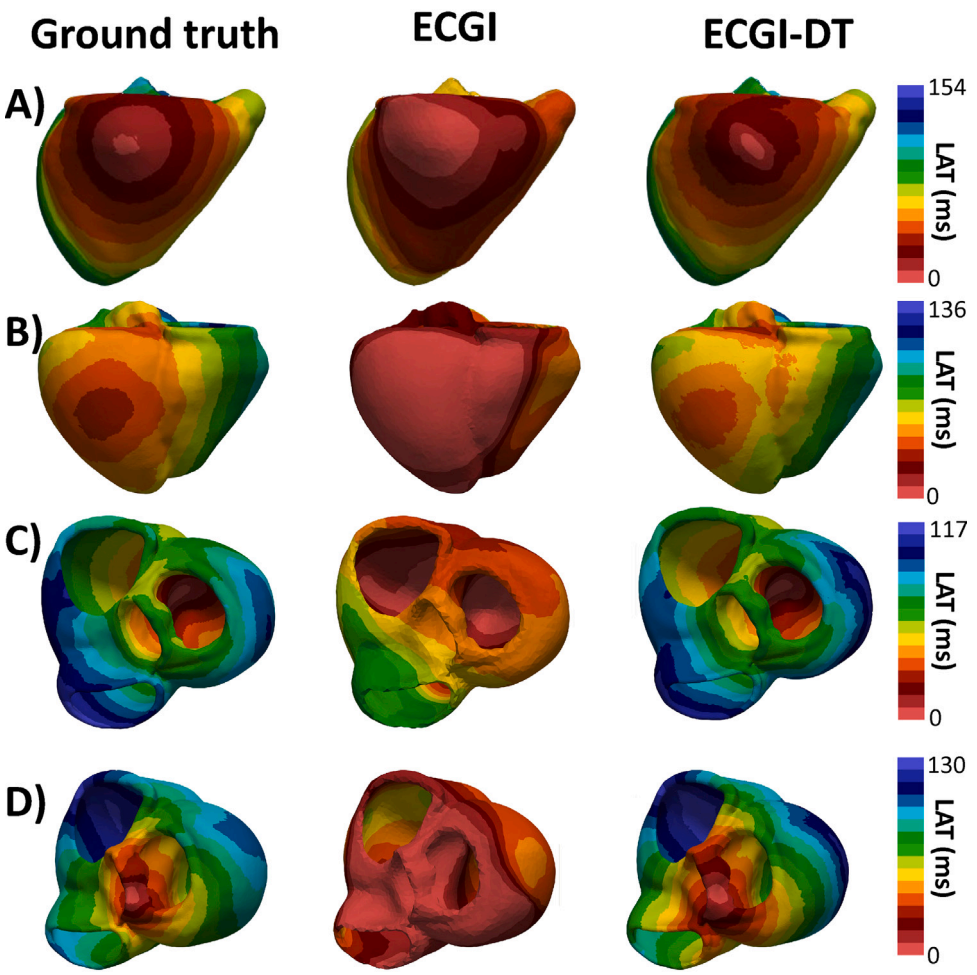

Fig. 4. Local activation time (LAT) maps for four different PVC locations. The first column depicts the ground truth LAT maps. The second column depicts the LAT map obtained from the ECGI potentials. The third column depicts the LAT map obtained from the ECGI-DT eikonal simulations. (A) PVC origin located at the endocardium of the right ventricular free wall. (B) PVC origin located at the endocardium of the left ventricular free wall. (C) PVC origin located at the septal wall of the left chamber. (D) PVC origin located at the aortic outflow tract.

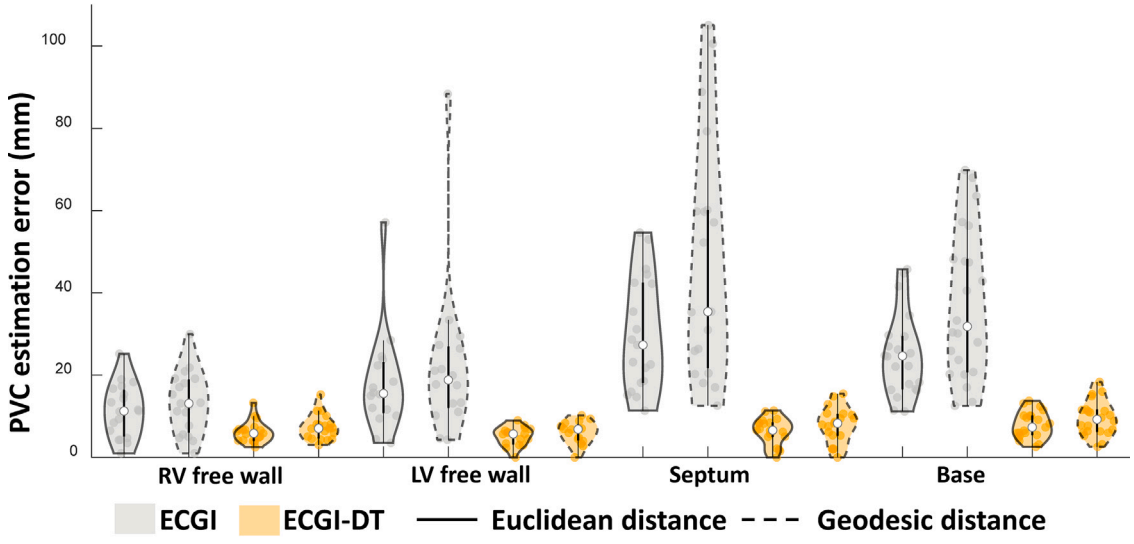

Fig. 5. Boxplot showing the Euclidean and geodesic error of estimation of PVC origin for four regions of the ventricles.

B.12). The mean RMSE value was 0.47 ± 0.43 mV and a maximum RMSE value was 0.90 mV for all cases (Fig. 8). It is worth noting that the maximum values of RMSE are located outside the area of the precordial leads. A higher correlation was reached for PVCs originating from the RV free wall (Fig. 8 panel A). While PVCs originating from the LVOT had a discrepancy in lead V5 (Fig. 8 panel D).

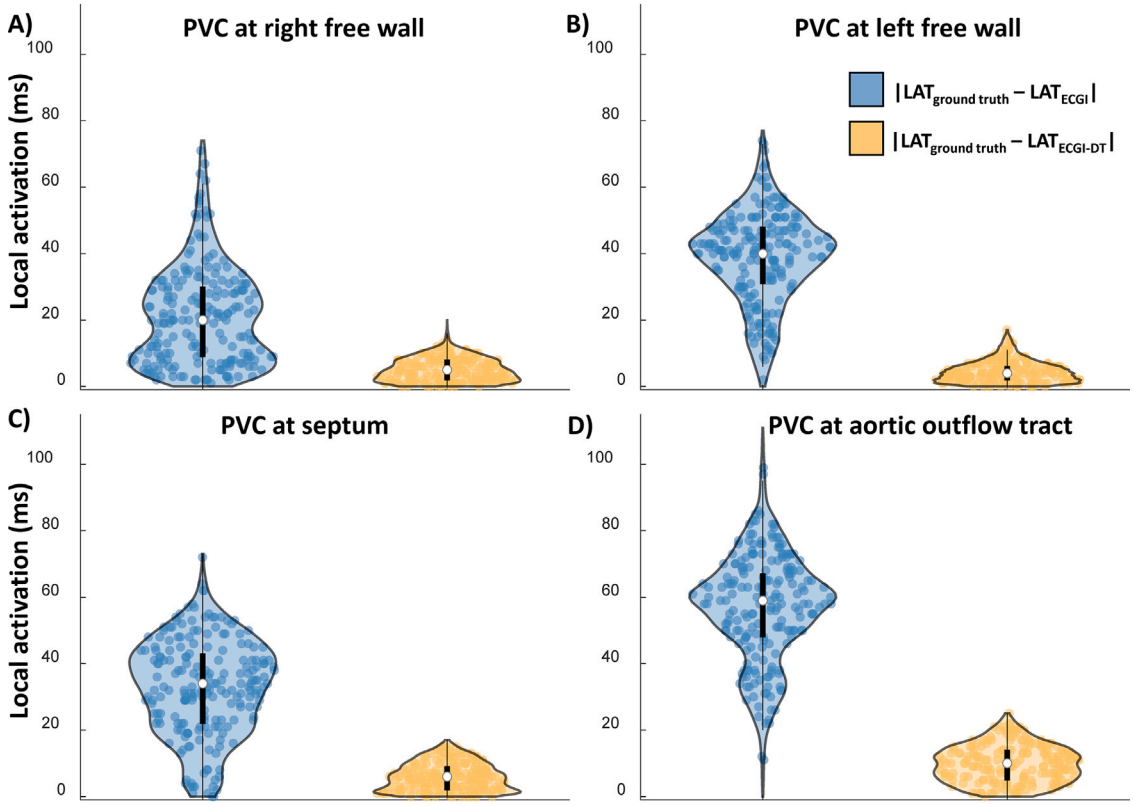

Fig. 6. Local activation time of ground truth, ECGI, and ECGI-DT for four different PVC locations.

Additionally, the proposed algorithm was further tested by adding white Gaussian noise at different SNR to the BSPM. From 40 to 0 dB of SNR, the error remained constant (7.81 ± 3.82 mm). We observed that the proposed algorithm proved to be robust to noise in the BSPM signals.

The proposed ECGI-DT algorithm was proven to be robust against uncertainty in the underlying conduction velocity with a variance that was 7.25 times smaller than ECGI. The variance of the mean error for all CVs for ECGI was 150.18 mm^2 and 20.69 mm^2 for ECGI-DT. Regional differences for all CVs can be observed in Fig. 9. The mean error locating PVCs increased to 9.36 ± 5.08 mm, 8.40 ± 4.15 mm, 9.54 ± 6.71 mm, and 20.78 ± 17.76 mm for 1.0, 0.8, 0.6, and 0.4 m/s, respectively (Fig. 9). In addition, ECGI mean error ranged from 35.77 ± 25.49 mm to 48.69 ± 32.69 mm for 1.0 and 0.4 m/s, respectively. When CV was known, ECGI-DT mean error at the RV free wall was 5.48 ± 2.96 mm. However, when CV varied, the mean error ranged from 11.90 ± 5.87 mm to 25.72 ± 20.73 mm for 1.0 and 0.4 m/s, respectively.

In addition, as a proof of concept, we tested the ECGI-DT in a patient diagnosed with a PVC in the LV free wall where the electroanatomical LAT map indicated the origin of the PVC (Fig. 10 panel A). ECGI-DT was able to locate the PVC origin with an error of 15.52 mm compared to ECGI where the error was 36.76 mm (Fig. 10 panel B). Moreover, both ECGI and ECG-DT estimated the location of the PVC at the epicardial site.

4. Discussion

In this study, we present a combined approach of ventricular digital twins and ECGI (ECGI-DT) that is capable of accurately locating the origin of PVCs. Additionally, the digital twin provides details about the electrical propagation through the ventricular myocardium. Moreover, the proposed algorithm can be used in real-world scenarios to plan ablation procedures of PVCs due to the reduced computational time needed to obtain a ventricular digital twin from ECGI compared to the current electroanatomical mapping strategies.

4.1. Location of PVCs using ECGI

Several studies have shown the potential of ECGI to estimate the origin of a PVC [15–18,60]. The range of ECGI mean error estimation in the literature ranges from 3.0 mm to 43.0 mm [16,20,61]. ECGI-DT achieved a mean error of 7.81 ± 3.82 mm, within the values reported in the literature. In this we showed that ECGI is useful for PVCs that originated at the right ventricular free wall where ECGI-DT have a similar precision. Dogrusoz et al. reported a mean Euclidean distance error to estimate PVCs origin, which varies depending on the used source model (dipole-based or potential-based). The mean Euclidean distance error reported range was 25.2 mm to 33.0 mm for a dipole-based source model and 13.9 mm to 39.2 mm for the potential-based source model [16]. Furthermore, Ondrusova et al. using an equivalent single layer source model, reported a mean Euclidean distance of 28.8 ± 11.9 mm, which agrees with the ECGI mean error in our study [17]. Additionally, Duchateau et al. reported a mean error of 75.7 ± 38.1 mm for estimating more than one primary epicardial breakthrough with ECGI compared with epicardial electroanatomical mapping [60]. However, in the presence of one epicardial breakthrough, the mean error was 52.2 ± 34.2 mm which agrees with our ECGI values for the RV and LV free wall (Fig. 3). The proposed ECGI-DT improved the estimation of a PVC origin by decreasing the mean error for different regions of the ventricle (Fig. 5). Moreover, Ogawa et al. [62] proposed a method to locate the area with respect to the pulmonary outflow tract (left cusp, right cusp, and anterior cusp) where the PVC triggers. The error of PVCs located close to the left cusp, which can be compared to the right free wall in this study, was 4.59 ± 8.54 mm. The error of ECGI-DT for the right free wall was 7.57 ± 2.96 mm mean value is higher but has a smaller standard

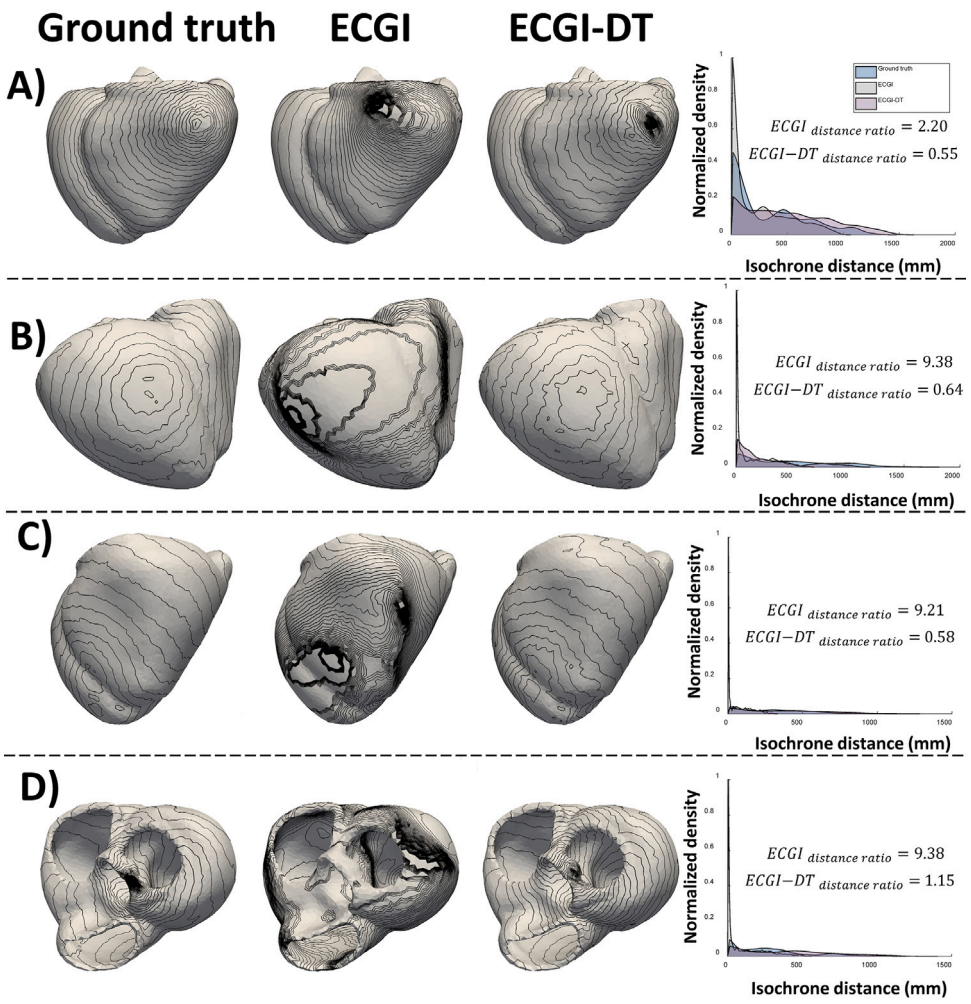

Fig. 7. Local activation time isochrones for four different PVC locations and the normalized isochrone density for ground truth, ECGI and ECGI-DT local activation time. (A) PVC located at the right ventricular free wall. (B) PVC located at the left ventricular free wall. (C) PVC located at the septum. (D) PVC located at the aortic outflow tract.

deviation which indicates a higher accuracy compared to the method proposed by Ogawa et al. [62].

Additionally, using different models of artificial intelligence, several studies were able to locate PVC origin [20–22]. Zhao et al. evaluated different machine learning models to identify the left or right ventricular outflow tract from where the PVC was originated using a random forest tree model [21]. The authors showed that the classifier was able to predict the PVC's origin, left or right ventricular outflow tract, with an accuracy of 94%. The proposed ECGI-DT showed that in all cases it was able to correctly identify the origin of the PVC at the left or right ventricular outflow tract. Moreover, Monacci et al. and Pilia et al. used eikonal models to simulate the ventricular electrophysiology and used universal coordinate system to generate a dataset to train an deep learning model to locate PVCs [20,22]. Interestingly, our approached also used a universal coordinate system and first principles models to estimate the PVC location based on ECGI. Artificial intelligence PVC location seem to have a higher accuracy (3 mm [20] and 4.06 mm [22]) compared to our ECGI-DT approach (7.81 ± 3.82 mm) perhaps due to the size of the database. One of the main difference with our proposed method is the higher number of simulated data used to train the algorithms.

Moreover, we showed that the proposed methodology was robust to changes in CV (Fig. 9). The maximum error for an unknown CV was 20.78 ± 17.76 mm for a CV of 0.4 m/s compared against the database which comprised simulations with a CV of 0.7 m/s. Additionally, ECGI-DT LAT maps have a maximum mean error in the LAT of 6.37 ± 9.23 ms for a PVC located in the LVOT and a maximum absolute error of 15 ms. The maximum absolute error in the proposed ventricular ECGI-DT could come from the eikonal model ignoring the source–sink mismatch, bath loading effects, high wavefront curvatures, and wavefront collision on CV [31,49,63–66]. Despite the eikonal model limitations, the simulations offer a reasonably good estimate of wave propagation in the absence of anatomical or structural remodeling. In addition, ECGI LAT maps are prone to create artificial lines of block [25,51,67]. The proposed ECGI-DT provides a LAT map with no artificial line of blocks as compared to ECGI (Fig. 7).

4.2. Ventricular digital twins

In this study, we present a workflow to create ventricular digital twins from ECGI data. Gillette et al. have shown that it is feasible to create cardiac digital twins using information from the 12-lead ECG [27]. Moreover, Gillette et al. showed a good qualitative match of the 12-lead ECG as a result of their minimization loss function. We showed that ECGI-DT can reproduce the BSPM of the ground truth and obtain a mean CC up to 0.80 of the precordial leads within a feasible time to be used in real-world applications by obtaining the BSPM and ECGI LATs of a patient. Additionally, Krummen et al. proposed the creation of a database that consists of computational models with different focal activity and other complex mechanisms such as ventricular fibrillation [68]. For the localization of PVCs, the authors reported a median error of 11 mm (interquartile range, 5–21 mm) compared to the

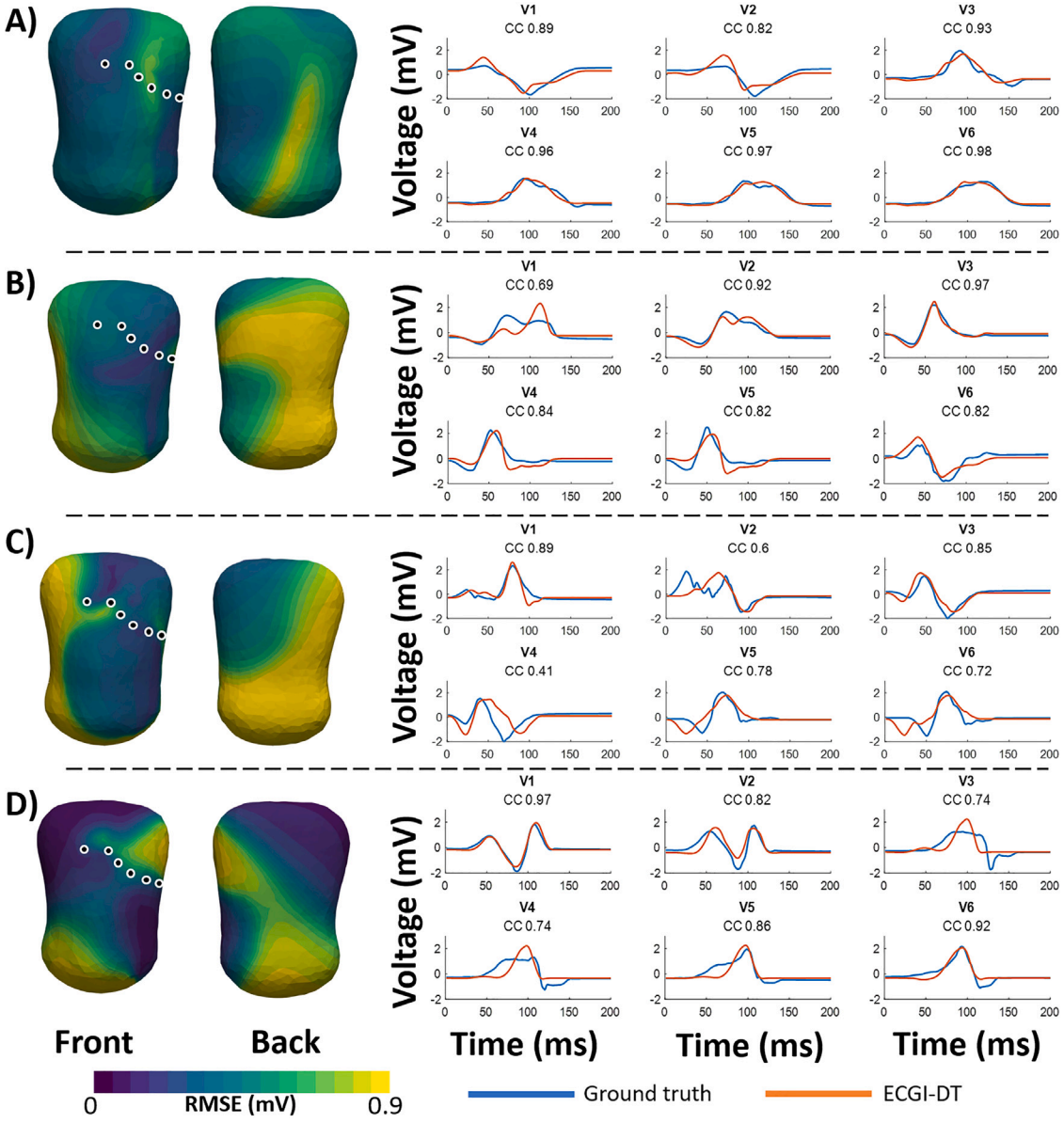

Fig. 8. Body surface potential root mean square error (RMSE) and signals at the position of standard precordial leads for four different PVC location. (A) ECGI-DT for a PVC located at the right ventricular free wall. (B) ECGI-DT for a PVC located at the left ventricular free wall. (C) ECGI-DT for a PVC located at the septum. (D) ECGI-DT for a PVC located at the aortic outflow tract.

location determined using electroanatomical maps to estimate PVCs. Our ECGI-DT approach had a mean error of 5.48 ± 2.96 mm for PVCs originated at the ventricular free wall, which is smaller to the error reported by Krummen et al. [68].

The creation of the ventricular digital twin was based on eikonal simulations and a transfer matrix to compute the BSPM for real-world applications in a feasible time. Potyagaylo et al. showed that a fastest route algorithm and forward problem solution using a transfer matrix can be used to solve the inverse problem and estimate the PVC origin with a mean error of less than 10 mm [35]. The proposed ECGI-DT is in agreement with the values reported by Potyagaylo et al. [35] with a mean error of 7.81 ± 3.82 mm. Additionally, ECGI-DT achieved smaller errors at the left ventricular summit and right ventricular apex where Potyagaylo et al. [35] reported a maximum error of 60 mm. Our ECGI-DT approach have a maximum error at the ventricular base of 18.35 mm. Additionally, we tested the proposed approach using a set of additional evaluation simulations with different conduction velocities. ECGI-DT proved to perform well for higher values of CVs, while for slower values of CVs, ECGI-DT mean error increased (Fig. 9 panel D).

Moreover, a coherent activation sequence produced by a PVC was obtained (Fig. 4), while ECGI gave non-coherent PVC activation sequences due to the smoothing effect of the regularization used to solve the ill-posed inverse problem as described by Schuler et al. [51] and shown previously using in vivo experiments [25,67]. However, we considered only homogeneous tissue without any local functional or structural remodeling, which could introduce real lines of block in LAT maps. The current implementation of ECGI-DT would not be able to capture any line of block produced by the presence of local functional or structural remodeling in the ventricular tissue [63].

4.3. Clinical outlook

The integration of ECGI-DT technology in the clinical management of PVCs can represent a major step in cardiology, creating a new paradigm in personalized cardiac care. Our approach, merging ECGI with the concept of cardiac digital twins, offers enhanced precision in diagnosing PVCs compared to ECGI alone (Fig. 10 panel B). ECGI-DT was able to identify the PVCs originating from the left or right

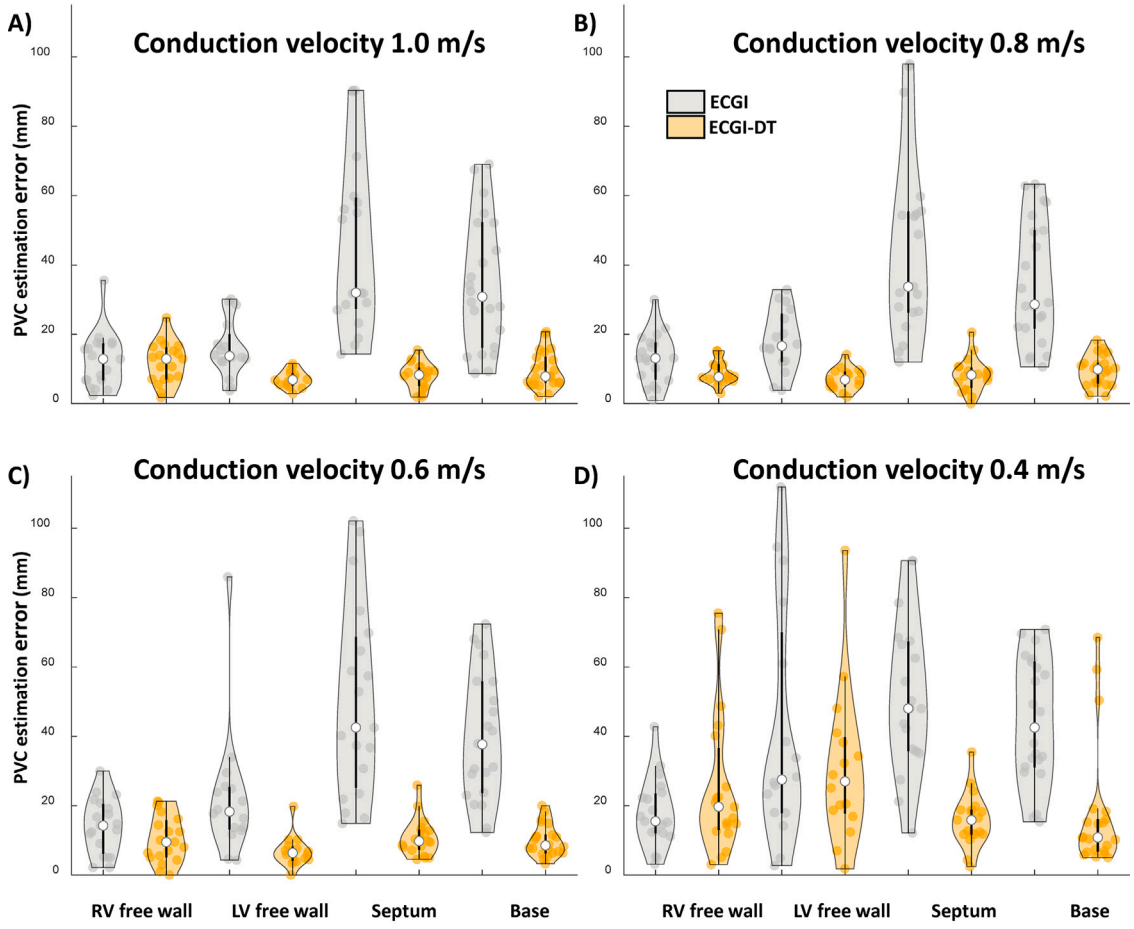

Fig. 9. Violin plots showing ECGI-DT performance to locate PVCs for four different conduction velocities. ECGI-DT was robust against higher conduction velocity and the error increased for low conduction velocity (0.4 m/s). ECGI in gray and ECGI-DT in orange. (A) Performance for CV 1 m/s. ECGI error is increased with a mean maximum error of 90 mm at the septum. (B) Performance for CV 0.8 m/s. ECGI error is increased with a mean maximum error of 98 mm at the septum. (C) Performance for CV 0.6 m/s. ECGI error is increased with a mean maximum error of 102 mm at septum. (D) Performance for CV 0.4 m/s. ECGI error is increased with a mean maximum error of 112 mm at the left ventricular free wall. Additionally, ECGI-DT was affected by a decrease in conduction velocity with a maximum mean error of 21 mm at the left ventricular free wall.

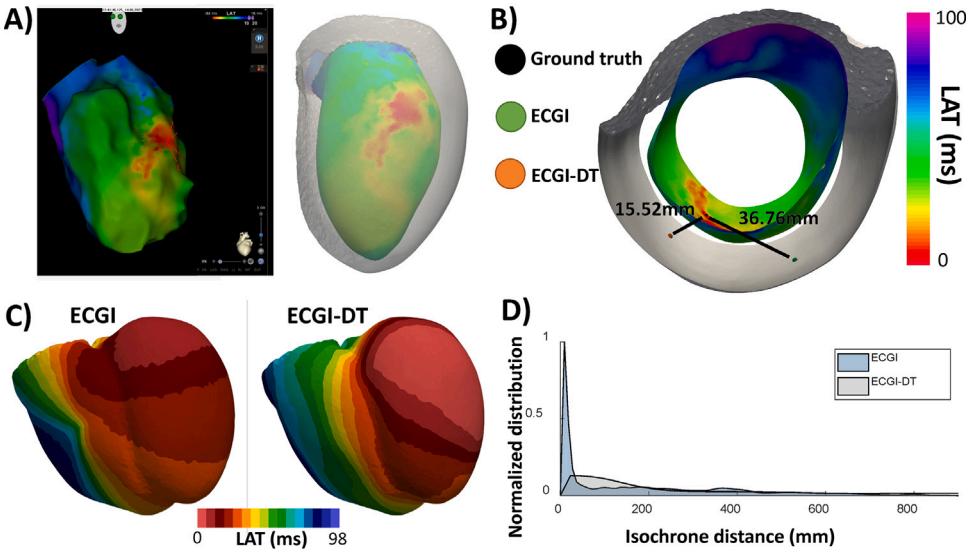

Fig. 10. ECGI-DT proof of concept using clinical data. Patient diagnose with a premature ventricular contraction at the left ventricular free wall. (A) Endocardial local activation time map and its respective coregistration to simulation geometry. (B) The earliest activation site was determined by finding the minimum in the endocardial local activation time map. ECGI-DT had a higher accuracy to determine the location of the premature ventricular contraction compared with ECGI. (C) ECGI and ECGI-DT local activation time maps. (D) Comparison of the normalized density of isochrones in the local activation time maps of both ECGI and ECGI-DT.

ventricular chamber and PVCs originating from the endocardial or epicardial site. By improving the accuracy of pinpointing the origin of PVCs, ECGI-DT facilitates more effective and tailored treatment strategies, improving the therapeutic landscape for patients suffering from PVCs. The ability of ECGI-DT to provide detailed insights into myocardial propagation and LATs enhances diagnostic accuracy and augments the efficacy of catheter ablation procedures, reducing the associated risks (Fig. 10 panel C). Svehlikova et al. [19,61] showed the potential of ECGI to localize the origin of the PVC and the importance of signal processing in clinical data. The evaluation in fourteen patients showed that removing the offset of the torso potentials reduce the localization error to a range between 1–2 mm [19]. Therefore, signal acquisition and preprocessing must be taken into account when thinking of integrating ECGI in the clinical practice.

New technologies have shown the potential to decrease ablation procedure times and radiation exposure [12,13]. To integrate the proposed ECGI-DT methodology into routine clinical practice, we envision it as a complementary tool for pre-procedural planning in patients undergoing catheter ablation for PVCs. Specifically, the ECGI-DT workflow could be utilized in cases where traditional 12-lead ECG or standard ECGI approaches yield ambiguous localization, such as PVCs originating from the septum, outflow tracts, or other complex regions. By combining ECGI-DT-derived localization with conventional mapping strategies, clinicians could refine ablation targets and optimize procedural planning. This approach may reduce reliance on extensive intra-procedural mapping, thereby potentially decreasing overall procedure time, minimizing radiation exposure, and improving patient outcomes. In the future, as ECGI-DT technology advances, the workflow could be further streamlined for clinical environments. For instance, integrating software with existing ECGI mapping systems, such as Acorys, could enable efficient patient-specific modeling. Additionally, expanding and standardizing precomputed digital twin databases would reduce computational demands, facilitating rapid deployment in clinical settings. These steps, coupled with rigorous clinical validation, would ensure the practical and effective integration of ECGI-DT into routine workflows for managing complex arrhythmias. Furthermore, ECGI-DT holds the potential to significantly advance personalized medicine in cardiology. By enabling clinicians to tailor treatments to the unique characteristics of each patient's cardiac electrophysiology, ECGI-DT paves the way for more patient-centric approaches, optimizing therapeutic outcomes while minimizing unnecessary interventions.

4.4. Limitations

While we showed the advantage of creating digital twins to enhance ECGI, several limitations must be considered. We only considered one ventricular geometry to create our database. Molero et al. [69] have shown the reduced effect of anatomical variability on ECGI. However, Mincholé et al. [29] showed that the ventricular anatomy impacts the ECG. Therefore, our dataset should be extended to consider the ventricular anatomical variability. Additionally, the number of models available our dataset can be extended as in Krummen et al. [68] and Pilia et al. [20] which can help to improve the accuracy of ECGI-DT. This could have an impact on the proposed methodology and should be further studied.

Moreover, we used a homogeneous model to obtain the transfer matrix and calculate the BSPM. Different studies reported that including heterogeneity of torso conductivity can improve the correlation of simulated BSPM with in vivo recordings [70] and of simulated data [32,71]. Thus, future work can include torso heterogeneity to obtain the transfer matrix and compute the forward problem. Different torso conductivity could potentially be obtained using impedance measurements [72–74]. In addition, we only considered the ventricles, but including the atria in the model can impact the estimation of the PVC. Therefore, future work should include a four-chamber model to include the impact of the atrial tissue in BSPM and the inverse reconstruction. This could potentially impact PVCs localization at the ventricular base.

The database created in this study did not include heterogeneity caused by remodeling of the ventricular myocardium. Including local functional or structural remodeling in the ventricular model have shown to introduce a source–sink mismatch and modify conduction [63–65]. The proposed ECGI-DT LAT maps did not consider any local functional or structural remodeling of the ventricular myocardium which produce lines of block. However, including models with local functional or structural remodeling can enhance the database and be able to identify areas with low conduction velocity.

We observed that the proposed methodology is robust to white Gaussian noise at different SNR. The influence of white Gaussian noise was not included in our PVC's database but can be extended. Additionally, this study did not consider the impact of reducing the number of electrodes when calculating ECGI. Ondrusova et al. [17] showed that the error in locating PVCs increased when the number of electrodes was reduced. Another aspect that could be explored is the impact of real-world artifacts such as electrode misplacement or other clinical factors that could influence the acquisition of the body surface potentials. Gillette et al. [27] showed that the 12-lead ECG was sufficient to create a digital twin and can be further studied when using ECGI information as a starting point for creating a ventricular digital twin.

Additionally, as a proof of concept, we tested ECGI-DT in one patient. Future research can include more patients, including electroanatomical mapping and ECGI. Both mapping modalities held the potential to quantitatively measure the accuracy of locating PVCs using ECGI and our proposed ECGI-DT.

4.5. Conclusion

In conclusion, we present a methodology that combines ECGI and digital twins to enhance the accuracy of locating the origin of PVCs. In addition, thanks to the developed digital twin, we provide LAT maps with no artificial line of blocks compared to ECGI LAT maps.

CRediT authorship contribution statement

Jorge Sánchez: Writing – review & editing, Writing – original draft, Software, Data curation, Conceptualization. **Inés Llorente-Lipe:** Writing – review & editing, Software, Data curation. **Cristian Barrios Espinosa:** Writing – review & editing, Software. **Axel Loewe:** Writing – review & editing, Software. **Ismael Hernández-Romero:** Writing – review & editing. **Jorge Vicente-Puig:** Writing – review & editing. **Santiago Ros:** Data curation. **Felipe Atienza:** Data curation. **Alejandro Carta-Bergaz:** Data curation. **Andreu M. Climent:** Writing – review & editing, Conceptualization. **Maria S. Guillem:** Writing – review & editing, Conceptualization.

Declaration of competing interest

The authors declare the following financial interests/personal relationships which may be considered as potential competing interests: Jorge Sánchez Arciniegas reports financial support was provided by Universitat Politècnica de València. Maria Salud Guillem Sánchez reports financial support was provided by Spain Ministry of Science and Innovation. Andreu Climent reports a relationship with Corify Care that includes: board membership and equity or stocks. Maria Guillem reports a relationship with Corify Care that includes: board membership and equity or stocks. Ismael Hernandez reports a relationship with Corify Care that includes: employment and equity or stocks. Felipe Atenza reports a relationship with Corify Care that includes: board membership and equity or stocks. If there are other authors, they declare that they have no known competing financial interests or personal relationships that could have appeared to influence the work reported in this paper.

Acknowledgments

This work was supported by grants PLEC2021-007614 funded by MCIN, Spain/AEI/10.13039/501100011033 and by "European Union NextGenerationEU/PRTR". This was supported by grant RYC2018-024346-I and by "ESF Investing in your future, Spain". This project has received funding from the European Union's Horizon 2020 research and innovation programme under the Marie Skłodowska-Curie grant agreement No. 860974. This work was supported by the Leibniz ScienceCampus, Germany "Digital Transformation of Research" with funds from the programme "Strategic Networking in the Leibniz Association". This research was supported by Deutsche Forschungsgemeinschaft, Germany (DFG, German Research Foundation) under grant LO 2093/9-1.

Appendix A. Extended cobiveco coordinates

We extended the Cobiveco coordinate system to include a detailed anatomical base of the ventricle. The extension was done by including label at the surface and at the volume of the mesh (Fig. A.11 panel A). First, using the volume labels we take out the right ridge between the right pulmonary outflow track and the tricuspid valve orifice. We also remove the ridge of the aortic outflow tract from the left ventricle. Second, we calculate the transventricular (tv), transmural (tm) as

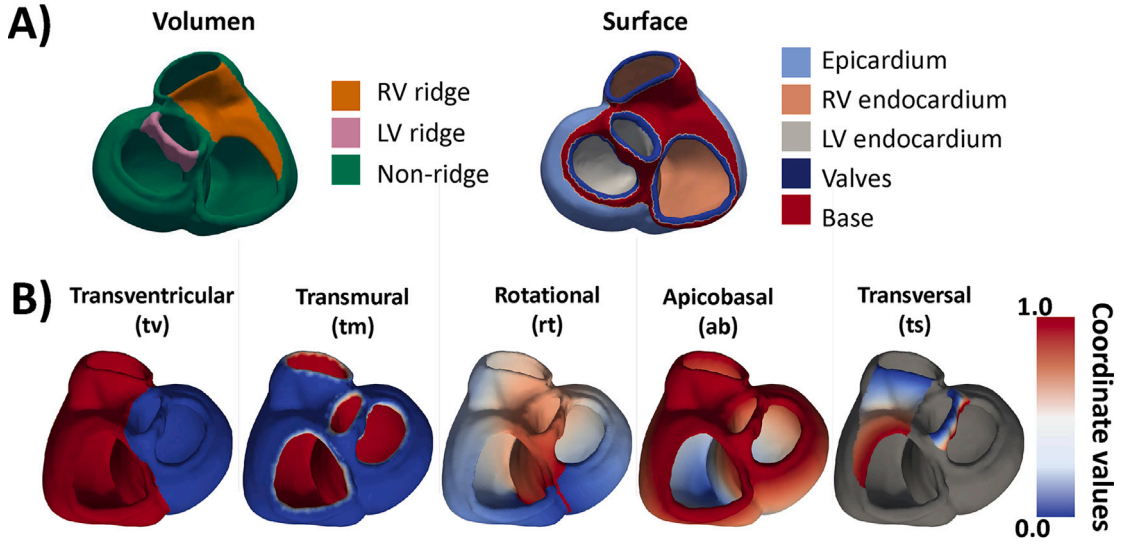

Fig. A.11. Extended Cobiveco in a detailed anatomical ventricular geometry. (A) Input labels in at the volume and surface of the ventricular mesh. (B) Result of the extended Cobiveco coordinates.

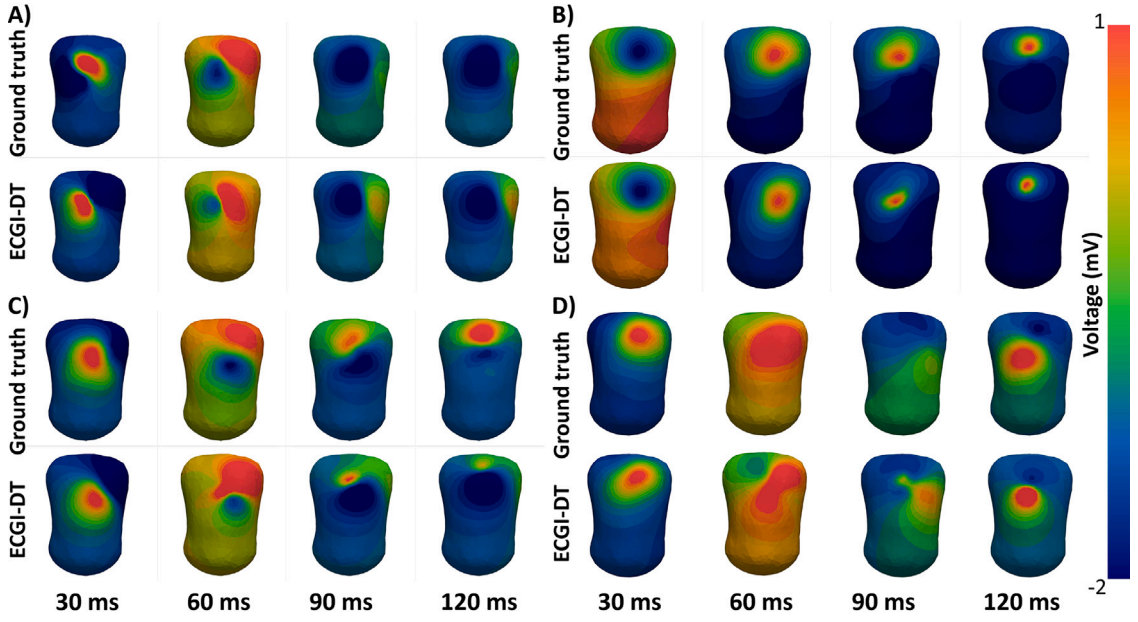

Fig. B.12. Snapshot of the body surface potential map for four different PVC locations. (A) PVC located at the right ventricular free wall. (B) PVC located at the left ventricular free wall. (C) PVC located at the septum. (D) PVC located at the aortic outflow tract.

described in [56]. Third, we calculate the rotational (rt) coordinate as described in the original Cobiveco formulation and we added the values at the boundaries of the ridges and solve the Laplace equation to have a continuous solution for the rotational coordinate. Fourth, to compute the apico-basal (ab) coordinate we used the same approach as in the original Cobiveco approach. Fifth, we added a scalar field at ridge of the aortic outflow tract and at the right pulmonary outflow track and the tricuspid valve orifice. The scalar field is call the transversal (ts) field. The scalar field ts is computed by setting boundary conditions to solve the Laplace equation. The boundary conditions were set boundary of the ridges, 0 was set to all points located at the boundary close to the pulmonary or aortic orifice and 1 was set to all points located at the boundary close to the tricuspid or mitral valve orifice. The new ts coordinate helps to better identify points located in this areas which the rt coordinate has values that cover big portions of areas. The resulting four extended Cobiveco coordinates are comparable to the original formulation of [56] and are depicted in Fig. A.11 panel B.

Appendix B. Body surface potential maps

We computed the body surface potential maps using boundary element methods as explained in Methods section. The resulting BSPMs for four different examples are shown in Fig. B.12.

References

[1] M.-S. Ahn, Current concepts of premature ventricular contractions, J. Lifestyle Med. 3 (1) (2013) 26–33.

[2] J.F. Huizar, A.Y. Tan, K. Kaszala, K.A. Ellenbogen, Clinical and translational insights on premature ventricular contractions and PVC-induced cardiomyopathy, Prog. Cardiovasc. Dis. 66 (2021) 17–27.

[3] G.M. Marcus, Evaluation and management of premature ventricular complexes, Circulation 141 (2020) 1404–1418.

[4] F.M. Ezzeddine, K.C. Siontis, Localization of outflow ventricular arrhythmias from the electrocardiogram: educated guess, science, or both? J. Interv. Card. Electrophysiol. 66 (2023) 1775–1777.

[5] D. Muser, M. Tritto, M.V. Mariani, A. Di Monaco, P. Compagnucci, M. Accogli, R.D. Ponti, F. Guarracini, Diagnosis and treatment of idiopathic premature ventricular contractions: A stepwise approach based on the site of origin, Diagnostics 11 (2021) 1840.

[6] P. Futyma, Ł. Zarębski, S. Chen, A. Enriquez, H. Pürerfellner, P. Santangeli, Risk assessment and management of outflow tract arrhythmias refractory to prior treatments, Curr. Cardiovasc. Risk Rep. 17 (2023) 21–26.

[7] L. Jia, L. Yue-Chun, J. Kang-Ting, Z. Na-Dan, L. Jia-Xuan, Z. Wen-Wu, Y. Peng-Lin, T. Ji-Fei, L. Jia-Feng, Premature ventricular contractions originating from the left ventricular septum: Results of radiofrequency catheter ablation in twenty patients, BMC Cardiovasc. Disord. 11 (2011) 27.

[8] F. Santoro, L. Di Biase, P. Hranitzky, J.E. Sanchez, P. Santangeli, A.P. Perini, J.D. Burkhardt, A. Natale, Ventricular fibrillation triggered by PVCs from papillary muscles: clinical features and ablation., J. Cardiovasc. Electrophysiol. 25 (2014) 1158–1164.

[9] S. Sikdar, D. Bera, K. Kumawat, A. Jahangir, P. Chakraborty, An unusual genetic observation in a case of short-coupled PVC-triggered ventricular fibrillation, JACC: Case Rep. 4 (2022) 101651.

[10] E.M. Cronin, F.M. Bogun, P. Maury, P. Peichl, M. Chen, N. Namboodiri, L. Aguinaga, L.R. Leite, S.M. Al-Khatib, E. Anter, A. Berruezo, D.J. Callans, M.K. Chung, P. Cuculich, A. d'Avila, B.J. Deal, P.D. Bella, T. Deneke, T.-M. Dickfeld, C. Hadid, H.M. Haqqani, G.N. Kay, R. Latchamsetty, F. Marchlinski, J.M. Miller, A. Nogami, A.R. Patel, R.K. Pathak, L.C.S. Morales, P. Santangeli, J.L. Sapp, A. Sarkozy, K. Soejima, W.G. Stevenson, U.B. Tedrow, W.S. Tzou, N. Varma, K. Zeppenfeld, 2019 HRS/EHRA/APHRS/LAHRS expert consensus statement on catheter ablation of ventricular arrhythmias, Hear. Rhythm. 17 (2020) e2–e154.

[11] L.S. Rosenthal, M. Mahesh, T.J. Beck, J. Saul, J.M. Miller, N. Kay, L.S. Klein, S. Huang, P. Gillette, E. Prystowsky, M. Carlson, R.D. Berger, J.H. Lawrence, P. Yong, H. Calkins, Predictors of fluoroscopy time and estimated radiation exposure during radiofrequency catheter ablation procedures, Am. J. Cardiol. 82 (1998) 451–458.

[12] L. Faroux, C. Daval, F. Lesaffre, T. Blanpain, J.-P. Chabert, A. Martin, M. Guinot, N. Luconi, M. Espinosa, P. Nazeyrollas, C. Tourneux, D. Metz, Physicians' exposure to radiation during electrophysiology procedures, J. Interv. Card. Electrophysiol. 55 (2) (2019) 233–237.

[13] X. Qiu, N. Zhang, Q. Luo, A. Liu, Y. Ji, J. Ye, C. Lin, T. Ling, K. Chen, W. Pan, J. Zhao, Q. Jin, L. Wu, Remote magnetic navigation facilitates the ablations of frequent ventricular premature complexes originating from the outflow tract and the valve annulus as compared to manual control navigation, Int. J. Cardiol. 267 (2018) 94–99.

[14] D. Penela, G. Falasconi, J.M. Carreño, D. Soto-Iglesias, J. Fernández-Armenta, J. Acosta, J. Martí-Almor, B. Benito, A. Bellido, A. Chauca, C. Scherer, D. Viveros, J. Alderete, E. Silva, A. Ordoñez, J. Francisco-Pascual, N. Rivas-Gandara, J. Meca-Santamaria, P. Franco, C.D. Lucia, H. Ali, R. Cappato, O. Cámara, P. Francia, A. Berruezo, A hybrid clinical and electrocardiographic score to predict the origin of outflow tract ventricular arrhythmias, J. Interv. Card. Electrophysiol. 66 (2023) 1877–1888.

[15] S. Misra, P. van Dam, J. Chrispin, F. Assis, A. Keramati, A. Kolandaivelu, R. Berger, H. Tandri, Initial validation of a novel ECGI system for localization of premature ventricular contractions and ventricular tachycardia in structurally normal and abnormal hearts, J. Electrocardiol. 51 (2018) 801–808.

[16] Y.S. Dogrusoz, N. Rasoolzadeh, B. Ondrusova, P. Hlivak, J. Zelinka, M. Tysler, J. Svehlikova, Comparison of dipole-based and potential-based ECGI methods for premature ventricular contraction beat localization with clinical data, Front. Physiol. 14 (2023).

[17] B. Ondrusova, P. Tino, J. Svehlikova, A two-step inverse solution for a single dipole cardiac source, Front. Physiol. 14 (2023).

[18] L. Parreira, P. Carmo, R. Marinheiro, D. Mesquita, M. Chmelevsky, A. Ferreira, L. Marques, J. Pinho, D. Chambel, S. Nunes, P. Amador, P. Gonçalves, H. Marques, R. Caria, P. Adragão, Assessment of wave front activation duration and speed across the right ventricular outflow tract using electrocardiographic imaging as predictors of the origin of the premature ventricular contractions: A validation study, J. Electrocardiol. 73 (2022) 68–75.

[19] J. Svehlikova, A. Pribilova, J. Zelinka, B. Ondrusova, K. Kromkova, P. Hlivak, R. Hatala, M. Tysler, The importance of ECG offset correction for premature ventricular contraction origin localization from clinical data, Meas. Sci. Rev. 22 (6) (2022) 246–252.

[20] N. Pilia, S. Schuler, M. Rees, G. Moik, D. Potyagaylo, O. Dössel, A. Loewe, Non-invasive localization of the ventricular excitation origin without patient-specific geometries using deep learning, Artif. Intell. Med. 143 (2023) 102619.

[21] W. Zhao, R. Zhu, J. Zhang, Y. Mao, H. Chen, W. Ju, M. Li, G. Yang, K. Gu, Z. Wang, H. Liu, J. Shi, X. Jiang, P. Kojodjojo, M. Chen, F. Zhang, Machine learning for distinguishing right from left premature ventricular contraction origin using surface electrocardiogram features, Hear. Rhythm. 19 (2022) 1781–1789.

[22] S. Monaci, K. Gillette, E. Puyol-Antón, R. Rajani, G. Plank, A. King, M. Bishop, Automated localization of focal ventricular tachycardia from simulated implanted device electrograms: A combined physics–AI approach, Front. Physiol. 12 (2021).

[23] J. Duchateau, F. Sacher, T. Pambrun, N. Derval, J. Chamorro-Servent, A. Denis, S. Ploux, M. Hocini, P. Jaïs, O. Bernus, M. Haïssaguerre, R. Dubois, Performance and limitations of noninvasive cardiac activation mapping, Hear. Rhythm. 16 (2019) 435–442.

[24] L.R. Bear, O. Bouhamama, M. Cluitmans, J. Duchateau, R.D. Walton, E. Abell, C. Belterman, M. Haissaguerre, O. Bernus, R. Coronel, R. Dubois, Advantages and pitfalls of noninvasive electrocardiographic imaging, J. Electrocardiol. 57 (2019) S15–S20.

[25] M.J. Cluitmans, P. Bonizzi, J.M. Karel, M. Das, B.L. Kietselaer, M.M. de Jong, F.W. Prinzen, R.L. Peeters, R.L. Westra, P.G. Volders, In vivo validation of electrocardiographic imaging, JACC: Clin. Electrophysiol. 3 (2017) 232–242.

[26] A. Loewe, P. Martínez Díaz, C. Nagel, J. Sánchez, Cardiac digital twin modeling, in: T. Jadczyk, G. Caluori, A. Loewe, K.S. Golba (Eds.), Innovative Treatment Strategies for Clinical Electrophysiology, Springer Nature Singapore, Singapore, 2022, pp. 111–134.

[27] K. Gillette, M.A. Gsell, A.J. Prassl, E. Karabelas, U. Reiter, G. Reiter, T. Grandits, C. Payer, D. Štern, M. Urschler, J.D. Bayer, C.M. Augustin, A. Neic, T. Pock, E.J. Vigmond, G. Plank, A framework for the generation of digital twins of cardiac electrophysiology from clinical 12-leads ECGs, Med. Image Anal. 71 (2021) 102080.

[28] L. Azzolin, M. Eichenlaub, C. Nagel, D. Nairn, J. Sanchez, L. Unger, O. Dössel, A. Jadidi, A. Loewe, Personalized ablation vs. conventional ablation strategies to terminate atrial fibrillation and prevent recurrence, EP Eur. 25 (2023) 211–222.

[29] A. Mincholé, E. Zacur, R. Ariga, V. Grau, B. Rodriguez, MRI-based computational torso/biventricular multiscale models to investigate the impact of anatomical variability on the ECG QRS complex, Front. Physiol. 10 (2019).

[30] C. Nagel, C.B. Espinosa, K. Gillette, M.A. Gsell, J. Sanchez, G. Plank, O. Dossel, A. Loewe, Comparison of propagation models and forward calculation methods on cellular, tissue and organ scale atrial electrophysiology, IEEE Trans. Biomed. Eng. 70 (2023) 511–522.

[31] A. Neic, F.O. Campos, A.J. Prassl, S.A. Niederer, M.J. Bishop, E.J. Vigmond, G. Plank, Efficient computation of electrograms and ECGs in human whole heart simulations using a reaction-eikonal model, J. Comput. Phys. 346 (2017) 191–211.

[32] D.U. Keller, F.M. Weber, G. Seemann, O. Dössel, Ranking the influence of tissue conductivities on forward-calculated ecgs, IEEE Trans. Biomed. Eng. 57 (2010) 1568–1576.

[33] M. Potse, B. Dube, A. Vinet, R. Cardinal, A comparison of monodomain and bidomain propagation models for the human heart, in: 2006 International Conference of the IEEE Engineering in Medicine and Biology Society, IEEE, 2006, pp. 3895–3898.

[34] S. Pezzuto, P. Kal'avský, M. Potse, F.W. Prinzen, A. Auricchio, R. Krause, Evaluation of a rapid anisotropic model for ECG simulation, Front. Physiol. 8 (2017).

[35] D. Potyagaylo, O. Dossel, P. van Dam, Influence of modeling errors on the initial estimate for nonlinear myocardial activation times imaging calculated with fastest route algorithm, IEEE Trans. Biomed. Eng. 63 (2016) 2576–2584.
[36] C. Rodero, M. Strocchi, M. Marciniak, S. Longobardi, J. Whitaker, M.D. O'Neill, K. Gillette, C. Augustin, G. Plank, E.J. Vigmond, P. Lamata, S.A. Niederer, Linking statistical shape models and simulated function in the healthy adult human heart, PLoS Comput. Biol. 17 (2021) e1008851.
[37] R. Molero, J.M.S. Torro, N.M. Alzamora, A.M. Climent, M.S. Guillem, Higher reproducibility of phase derived metrics from electrocardiographic imaging during atrial fibrillation in patients remaining in sinus rhythm after pulmonary vein isolation, Comput. Biol. Med. 139 (2021) 104934.
[38] S. Qian, S. Monaci, C. Mendonca-Costa, F. Campos, P. Gemmell, H.A. Zaidi, R. Rajani, J. Whitaker, C.A. Rinaldi, M.J. Bishop, Additional coils mitigate elevated defibrillation threshold in right-sided implantable cardioverter defibrillator generator placement: a simulation study, Europace 25 (2023).
[39] J.D. Bayer, R.C. Blake, G. Plank, N.A. Trayanova, A novel rule-based algorithm for assigning myocardial fiber orientation to computational heart models, Ann. Biomed. Eng. 40 (2012) 2243–2254.
[40] D. Durrer, R.T. van Dam, G.E. Freud, M.J. Janse, F.L. Meijler, R.C. Arzbaecher, Total excitation of the isolated human heart., Circulation 41 (1970) 899–912.
[41] P. Taggart, P.M. Sutton, T. Opthof, R. Coronel, R. Trimlett, W. Pugsley, P. Kallis, Inhomogeneous transmural conduction during early ischaemia in patients with coronary artery disease, J. Mol. Cell. Cardiol. 32 (2000) 621–630.
[42] C.M. Costa, F.O. Campos, A.J. Prassl, R.W.D. Santos, D. Sanchez-Quintana, E. Hofer, G. Plank, A finite element approach for modeling micro-structural discontinuities in the heart, in: Proceedings of the Annual International Conference of the IEEE Engineering in Medicine and Biology Society, EMBS, 2011, pp. 437–440.
[43] J. Tomek, A. Bueno-Orovio, E. Passini, X. Zhou, A. Minchole, O. Britton, C. Bartolucci, S. Severi, A. Shrier, L. Virag, A. Varro, B. Rodriguez, Development, calibration, and validation of a novel human ventricular myocyte model in health, disease, and drug block, ELife 8 (2019).
[44] G. Plank, A. Loewe, A. Neic, C. Augustin, Y.-L. Huang, M.A. Gsell, E. Karabelas, M. Nothstein, A.J. Prassl, J. Sánchez, G. Seemann, E.J. Vigmond, The openCARP simulation environment for cardiac electrophysiology, Comput. Methods Programs Biomed. 208 (2021).
[45] openCARP consortium, C. Augustin, P.M. Boyle, V. Loechner, R. Colin, A. Huppé, M. Gsell, M. Houillon, Y.-L.C. Huang, K.G. Hustad, E. Karabelas, A. Loewe, L. Myklebust, A. Neic, M. Nothstein, G. Plank, A. Prassl, J. Sánchez, G. Seemann, T. Stary, A. Thangamani, N. Tippmann, T. Trevisan Jost, E. Vigmond, E.M. Wülfers, M. Linder, Opencarp, 2023.
[46] C. Barrios Espinosa, J. Sánchez, S. Appel, S. Becker, J. Krauß, P. Martínez Díaz, L. Unger, M. Houillon, A. Loewe, A cyclical fast iterative method for simulating reentries in cardiac electrophysiology using an eikonal-based model, Eng. Comput. (2025).
[47] C.B. Espinosa, J. Sánchez, O. Dössel, A. Loewe, Diffusion reaction eikonal alternant model: Towards fast simulations of complex cardiac arrhythmias, in: 2022 Computing in Cardiology (CinC), vol. 498, 2022, pp. 1–4.
[48] C.C. Mitchell, D.G. Schaeffer, A two-current model for the dynamics of cardiac membrane., Bull. Math. Biol. 65 (2003) 767–793.
[49] C. Nagel, S. Schuler, O. Dössel, A. Loewe, A bi-atrial statistical shape model for large-scale in silico studies of human atria: Model development and application to ECG simulations, Med. Image Anal. 74 (2021) 102210.
[50] M. Stenroos, V. Mäntynen, J. Nenonen, A Matlab library for solving quasi-static volume conduction problems using the boundary element method, Comput. Methods Programs Biomed. 88 (2007) 256–263.
[51] S. Schuler, M. Schaufelberger, L.R. Bear, J.A. Bergquist, M.J.M. Cluitmans, J. Coll-Font, O.N. Onak, B. Zenger, A. Loewe, R.S. MacLeod, D.H. Brooks, O. Dossel, Reducing line-of-block artifacts in cardiac activation maps estimated using ECG imaging: A comparison of source models and estimation methods, IEEE Trans. Biomed. Eng. 69 (2022) 2041–2052.
[52] A. Kalinin, D. Potyagaylo, V. Kalinin, Solving the inverse problem of electrocardiography on the endocardium using a single layer source, Front. Physiol. 10 (2019).
[53] P.C. Hansen, The L-Curve and its use in the numerical treatment of inverse problems, in: P. Johnston (Ed.), Invite Computational Inverse Problems in Electrocardiology, WIT Press, 2000.
[54] I. Hernández-Romero, C.F. Santos, C.H. Martín, A.M. Climent, M. de la Salud Guillem Sánchez, Local Conduction Velocity Estimation during Wavefront Collisions and Reentrant Scenarios, 2022.
[55] R.S. Antonio, E. Guasch, A. González-Ascaso, R. Jiménez-Arjona, A.M. Climent, M. Pujol-López, A. Doltra, F. Alarcón, P. Garre, A. Liberos, O. Trotta, L. Quinto, R. Borràs, E. Arbelo, I. Roca-Luque, F. Atienza, J. Brugada, F. Fernández-Avilés, M.S. Guillem, M. Sitges, J.M. Tolosana, L. Mont, Optimized single-point left ventricular pacing leads to improved resynchronization compared with multipoint pacing, Pacing Clin. Electrophysiol. 44 (2021) 519–527.
[56] S. Schuler, N. Pilia, D. Potyagaylo, A. Loewe, Cobiveco: Consistent biventricular coordinates for precise and intuitive description of position in the heart – with MATLAB implementation, Med. Image Anal. 74 (2021) 102247.
[57] J. Kennedy, R. Eberhart, Particle swarm optimization, in: Proceedings of ICNN'95 - International Conference on Neural Networks, vol. 4, IEEE, 1995, pp. 1942–1948.
[58] P. Hart, N. Nilsson, B. Raphael, A formal basis for the heuristic determination of minimum cost paths, IEEE Trans. Syst. Sci. Cybern. 4 (1968) 100–107.
[59] A.A. Hagberg, D.A. Schult, P.J. Swart, Exploring network structure, dynamics, and function using networkx, in: G. Varoquaux, T. Vaught, J. Millman (Eds.), Proceedings of the 7th Python in Science Conference, Pasadena, CA USA, 2008, pp. 11–15.
[60] J. Duchateau, M. Potse, R. Dubois, Spatially coherent activation maps for electrocardiographic imaging, IEEE Trans. Biomed. Eng. 64 (2017) 1149–1156.
[61] J. Svehlikova, M. Teplan, M. Tysler, Geometrical constraint of sources in noninvasive localization of premature ventricular contractions, J. Electrocardiol. 51 (3) (2018) 370–377.
[62] K. Ogawa, A. Hirata, Source localization and classification of pulmonary valve-originated electrocardiograms using volume conductor modeling with anatomical models, Biosensors 14 (10) (2024).
[63] F.O. Campos, Y. Shiferaw, R.W. dos Santos, G. Plank, M.J. Bishop, Microscopic isthmuses and fibrosis within the border zone of infarcted hearts promote calcium-mediated ectopy and conduction block, Front. Phys. 6 (2018) 1–14.
[64] E.J. Ciaccio, J. Coromilas, A.L. Wit, N.S. Peters, H. Garan, Source-sink mismatch causing functional conduction block in re-entrant ventricular tachycardia, JACC: Clin. Electrophysiol. 4 (2018) 1–16.
[65] P. Spector, Principles of cardiac electric propagation and their implications for re-entrant arrhythmias, Circulation: Arrhythmia Electrophysiol. 6 (2013) 655–661.
[66] N. Skupien, C.B. Espinosa, O. Dössel, A. Loewe, Refining the eikonal model to reproduce the influence of atrial tissue geometry on conduction velocity, Curr. Dir. Biomed. Eng. 8 (2) (2022) 133–136.
[67] L.R. Bear, J.A. Bergquist, E. Abell, H. Cochet, R.S. MacLeod, R. Dubois, Y. Serinagaoglu, Investigation into the importance of using natural PVCs and pathological models for potential-based ECGI validation, Front. Physiol. 14 (2023).
[68] D.E. Krummen, C.T. Villongco, G. Ho, A.A. Schricker, M.E. Field, K. Sung, K.A. Kacena, M.S. Martinson, K.S. Hoffmayer, J.C. Hsu, F. Raissi, G.K. Feld, A.D. McCulloch, F.T. Han, Forward-solution noninvasive computational arrhythmia mapping: The VMAP study, Circulation: Arrhythmia Electrophysiol. 15 (2022) E010857.
[69] R. Molero, A. González-Ascaso, A.M. Climent, M.S. Guillem, Robustness of imageless electrocardiographic imaging against uncertainty in atrial morphology and location, J. Electrocardiol. 77 (2023) 58–61.
[70] L.R. Bear, L.K. Cheng, I.J. LeGrice, G.B. Sands, N.A. Lever, D.J. Paterson, B.H. Smaill, Forward problem of electrocardiography, Circulation: Arrhythmia Electrophysiol. 8 (2015) 677–684.
[71] Y. Nakano, E.A. Rashed, T. Nakane, I. Laakso, A. Hirata, ECG localization method based on volume conductor model and Kalman filtering, Sensors 21 (13) (2021) 4275.
[72] A. Adler, A. Boyle, Electrical impedance tomography: Tissue properties to image measures, IEEE Trans. Biomed. Eng. 64 (11) (2017) 2494–2504.
[73] T. Doležal, M. Štumpf, Q. Hua, O. Franek, Measurement of electrical conductivity of human tissue: A feasibility study of a novel time-domain approach, Measurement 242 (2025) 115763.
[74] L.H.T. Okamura, L.H. Costa, G.C. Duran, A.K. Sato, E.K. Ueda, R.Y. Takimoto, T.C. Martins, M.S.G. Tsuzuki, Thorax and internal organs boundary geometries determination using convolutional neural networks in electrical impedance tomography, Eng. Appl. Artif. Intell. 136 (2024) 108918.